

Article

Pharmacogenomic Studies of Antiviral Drug Favipiravir

Victoria V. Shumyantseva ^{1,2,*} , Tatiana V. Bulko ¹, Alexey A. Chistov ¹, Ekaterina F. Kolesanova ¹
and Lyubov E. Agafonova ¹

¹ Institute of Biomedical Chemistry, Pogodinskaya Street, 10, Build 8, Moscow 119121, Russia; tanyabulko@mail.ru (T.V.B.); dobr14@yandex.ru (A.A.C.); ekolesanova@yandex.ru (E.F.K.); agafonovaluba@mail.ru (L.E.A.)

² Department of Biochemistry, Pirogov Russian National Research Medical University, Ostrovitianov Street, 1, Moscow 117997, Russia

* Correspondence: viktoria.shumyantseva@ibmc.msk.ru; Tel.: +7-4992465820

Abstract: In this work, we conducted a study of the interaction between DNA and favipiravir (FAV). This chemotherapeutic compound is an antiviral drug for the treatment of COVID-19 and other infections caused by RNA viruses. This paper examines the electroanalytical characteristics of FAV. The determined concentrations correspond to therapeutically significant ones in the range of 50–500 μM ($R^2 = 0.943$). We have shown that FAV can be electro-oxidized around the potential of +0.96 V \div +0.98 V (vs. Ag/AgCl). A mechanism for electrochemical oxidation of FAV was proposed. The effect of the drug on DNA was recorded as changes in the intensity of electrochemical oxidation of heterocyclic nucleobases (guanine, adenine and thymine) using screen-printed graphite electrodes modified with single-walled carbon nanotubes and titanium oxide nanoparticles. In this work, the binding constants (K_b) of FAV/dsDNA complexes for guanine, adenine and thymine were calculated. The values of the DNA-mediated electrochemical decline coefficient were calculated as the ratio of the intensity of signals for the electrochemical oxidation of guanine, adenine and thymine in the presence of FAV to the intensity of signals for the electro-oxidation of these bases without drug (S, %). Based on the analysis of electrochemical parameters, values of binding constants and spectral data, intercalation was proposed as the principal mechanism of the antiviral drug FAV interaction with DNA. The interaction with calf thymus DNA also confirmed the intercalation mechanism. However, an additional mode of interaction, such as a damage effect together with electrostatic interactions, was revealed in a prolonged exposure of DNA to FAV.

Keywords: favipiravir; electrochemistry; modified electrodes; DNA; drug/DNA interaction



Citation: Shumyantseva, V.V.; Bulko, T.V.; Chistov, A.A.; Kolesanova, E.F.; Agafonova, L.E. Pharmacogenomic Studies of Antiviral Drug Favipiravir. *Pharmaceutics* **2024**, *16*, 503. <https://doi.org/10.3390/pharmaceutics16040503>

Academic Editor: George P. Patrinos

Received: 28 February 2024

Revised: 22 March 2024

Accepted: 1 April 2024

Published: 7 April 2024



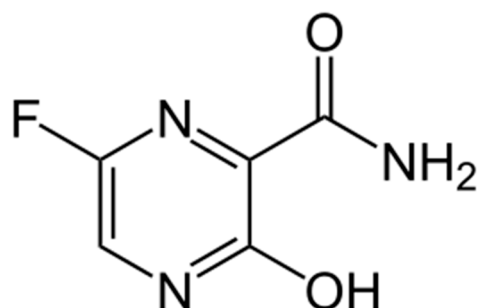
Copyright: © 2024 by the authors. Licensee MDPI, Basel, Switzerland. This article is an open access article distributed under the terms and conditions of the Creative Commons Attribution (CC BY) license (<https://creativecommons.org/licenses/by/4.0/>).

1. Introduction

Favipiravir's (6-fluoro-3-hydroxy-1,4-pyrazine-2-carboxamide, Scheme 1) (FAV) is rather broad antiviral activity has led to great interest being shown in it by the research community [1]. This synthetic analog of natural nucleobases shows efficacy against various RNA-containing viruses: orthomyxoviruses (human influenza type A, B and C viruses) [2–6], flaviviruses (Zika, dengue and West-Nile fever viruses) [7–9], arboviruses (Rift Valley, Crimean-Congo fever viruses) [10,11], arenaviruses [12], paramyxo-, alpha-, bunya-, and noroviruses [13,14]. FAV was found relatively efficient against such dangerous pathogens as Ebola fever [15] and rabies viruses [16].

FAV was shown to effectively inhibit the reproduction of human influenza viruses, including those resistant to neuraminidase and M2 protein inhibitors, as well as potentially dangerous swine and avian influenza viruses [4–6,17,18]. A number of clinical trials demonstrated FAV efficacy in treating infections caused by coronaviruses SARS-CoV, MERS and SARS-CoV2 [19–22]. However, in the course of clinical studies and observations, the side effects of FAV were revealed (nausea and vomiting, hyperuricemia, increased hepatic transaminases, neutro- and leukopenia, in some cases—cardiotoxicity and a number

of others) [6,19–24]. The results of FAV preclinical studies on small laboratory animals indicated its teratogenicity and embryotoxicity [6]. This imposes restrictions on the use of FAV medications in a number of patients. The side effects are mainly associated with the effect of this compound on the metabolism of nucleobases and potential mutagenicity by interacting with DNA [24].



Scheme 1. Chemical structure of favipiravir (6-fluoro-3-hydroxypyrazine-2-carboxamide).

FAV is a prodrug. It turns into the active compound 5'-ribosyl triphosphate FAV in human body cells [3,5,25–27]. This nucleotide analog can be recognized as a substrate by RNA-dependent RNA-polymerases from various viruses and can be incorporated in viral RNA as an analog of 5'-guanic acid (G) or, less likely, of 5'-adenylic acid (A), thus causing lethal mutations in the viral genome, behaving as a purine analog [28,29]. However, FAV also can form FAV:G and FAV:A pairs, and, in this case, FAV would behave as a pyrimidine analog [29]. This process is considered a principal mechanism of FAV activity against various viruses [28–31]. During influenza virus replication, FAV can also act as an inhibitor of viral RNA polymerase, causing the formation of truncated RNA chains [25,32]. DNA-dependent RNA polymerases do not recognize FAV ribosyl triphosphate as a substrate and do not incorporate it in transcribed RNA, thus establishing the base for selective effects of FAV on RNA-containing viruses [3].

FAV phosphoribosylation to ribosyl monophosphate nucleotide is catalyzed by hypoxanthine-guanine phosphoribosyl transferase [25–27]; the enzymes that are employed in the further phosphorylation up to ribosyl triphosphate FAV are unknown [27]. FAV conversion to the corresponding nucleotide proceeds much slower than in the case of natural nucleotides: monophosphoryl-ribosylation is 4700 times slower on average [26]. In addition, the rates of these conversions depend on cell types [33]. Hence, a substantial part of FAV that penetrates the cells may remain as the nucleobase, and this prodrug form can cause a part of its side effects. Therefore, it was of interest to study the possibility of interaction of FAV with cellular components at the molecular level. Taking into account base-pairing properties of FAV [29], its interaction with DNA by an intercalation between nucleobase residues in the double helix seems possible.

DNA plays an important role in a variety of biological processes such as gene transcription, mutagenesis and carcinogenesis. The interaction of a drug with DNA can help to understand the mechanisms and patterns of pharmacological chemicals actions and to screen DNA-targeting drugs.

Electroanalytical techniques provide useful insights into the mechanisms of the interactions of DNA with medications [34–39]. Electroanalysis has a triple function, registering the drug itself, DNA, and the DNA/drug complex. Scrutiny of the electrochemical signals of DNA or DNA/chemotherapeutic agent complex before and after binding can register the interaction and clarify the binding mechanism.

The goal of this research was to assess the impact of FAV as a remedy with a broad spectrum of antiviral action on the DNA molecule via the registration of electro-chemical oxidation signals of heterocyclic bases guanine, adenine, and thymine. The novelty of our research lies in the first investigation of FAV with dsDNA and ctDNA from a pharmacogenomics viewpoint.

2. Materials and Methods

2.1. Apparatus

In our experiments, we used two types of potentiostat/galvanostat, such as PGSTAT 12 Autolab (Metrohm Autolab, Utrecht, The Netherlands) with the GPES software (version 4.9.7) and a PalmSens potentiostat (PalmSens BV, Houten, The Netherlands) with PStTrace software (version 5.8). Electrochemical measurements were conducted at 20.0 °C. All experiments were performed in a supporting electrolyte—0.1 M potassium phosphate buffer with 50 mM NaCl (PBS, pH 7.4). For the registration of direct analysis of electrochemical dsDNA oxidation, the differential pulse voltammetry (DPV) method was used. The following optimized DPV parameters were used: potential range of 0.2–1.2 V, pulse amplitude of 0.025 V, potential step of 0.005 V, pulse duration of 50 ms, and modulation amplitude of 0.05 V. The square wave voltammetry (SWV) settings were as follows: potential range of 0–1.2 V, pulse amplitude of 0.005 V, potential step of 0.005 V, and frequency 10 Hz. Triplicated measurements were applied for electrochemical estimation of various DNA concentrations. These values were within 10–12% (the standard deviation, SD =10–12%), which satisfies the repeatability of the electrochemical installation when studying biological objects.

The UV–vis absorption spectra were registered with Cary 100 Scan spectrophotometer UV–Vis (Agilent Technologies, Inc., Santa Clara, CA, USA) with the software Cary WinUV version 3.00(182). The absorption spectra for FAV, DNA and the FAV/DNA complex were recorded in the range of 200–500 nm.

Commercially available screen-printed electrodes (SPEs) were obtained from Col-orElectronics, Moscow, Russia (<http://www.colorel.ru> (accessed on 1 February 2024)). The SPEs contained graphite working electrodes (geometric area 0.0314 cm²), auxiliary electrodes, and silver/silver chloride reference electrode (Ag/AgCl). All potentials were referred to the Ag/AgCl reference electrode.

2.2. Chemicals

“Medsintez” Ltd. (Moscow, Russia) kindly provided Favipiravir drug substance. Single-walled carbon nanotubes (SWCNT, diameter 1.6 ± 0.4 nm, length $> 5 \mu\text{m}$, surface area 1000 m²/g) TUBALL™ BATT H₂O, with water dispersion of 0.4%, stabilized by carboxymethylcellulose, were obtained from OCSIAL Ltd. (<https://ocsial.com>, (accessed on 1 February 2024)). Potassium phosphate monobasic ($\geq 99\%$), and potassium phosphate dibasic trihydrate ($\geq 99\%$) were purchased from Sigma-Aldrich. Sodium chloride (99.5%) was purchased from Acros Organics (Carlsbad, CA, USA). Double-stranded fish sperm DNA (dsDNA) as lyophilized powder was bought from Sigma-Aldrich (D 3159, Tokyo, Japan). Calf thymus DNA was obtained from Serva (Heidelberg, Germany). All other chemicals were of analytical grade and used without further purification. All aqueous solutions were prepared using Milli-Q water (18.2 MΩcm) purified with a Milli-Q water purification system by Millipore. The quality and purity of the DNA stock solution was checked by taking the absorbance ratio of A₂₆₀/A₂₈₀, which was found to be in the range of 1.8–1.9, indicating there is no contamination of protein in ds-DNA solution [39]. The stock solution of dsDNA (3 mg/mL) was prepared in 100 mM potassium phosphate buffer with 50 mM NaCl (PBS, pH 7.4) [40,41].

2.3. Preparation of Modified Electrode

To modify the surface of working electrodes with single-walled carbon nanotubes, we applied 2 μL of dispersion of SWCNT by drop casting. The commercial dispersion of SWCNT TUBALL™ BATT H₂O was preliminarily diluted 5 times in distilled water (named SPE/CNT; 0.75 ± 0.05 mg/mL). The concentration of SWCNT was chosen empirically as the best signal-to-noise ratio.

For surface modification with titanium oxide, the TiO₂ suspension (1 mg in 0.5 mL of H₂O:C₂H₅OH mixture, 1:1 *v/v* [42,43]) was sonicated for 1 h and a 2 μL aliquot of the suspension was pre-mixed with 2 μL of dispersion of SWCNT. SPE/CNT/TiO₂ was prepared by drop casting of 4 μL mixture of CNT and TiO₂ suspensions.

Electrodes SPE/CNT and SPE/CNT/TiO₂ stayed at room temperature until completely dried. Modified SPEs were used for a single measurement in order to avoid the blockage of the electrode surface by oxidation products of DNA or FAV.

For noncovalent immobilization of dsDNA, 60 µL of the dsDNA solution (1.5 mg/mL) prepared in PBS, with pH 7.4, was dropped onto the surface of the modified electrode and incubated for 15 min before measurements. For the investigation of DNA/drug interaction, a complex of DNA with FAV was formed at the constant concentration of DNA 1.5 mg/mL and specified concentrations of FAV, and was incubated 40 min before adsorption onto the electrode surface. DPV measurements were performed after 60 s deposition time.

A horizontal measurement regimen was used for all electrochemical experiments. A 60 µL drop of PBS was placed onto the SPEs to cover the surface of all three electrodes. Experiments were performed under aerobic conditions at room temperature (25 ± 3 °C). To assess the reproducibility of the results for each concentration, at least 3 electrodes were used and the standard deviation was calculated.

The calibration curve as kSD/b ($k = 3$ for the limit of detection, LOD, $b =$ slope) was employed for the calculation of LOD ($SD =$ standard deviation of the intercept) [44,45].

Linear plots for $1/(I_0 - I)$ depending on $1/[FAV]$ were used for the calculation of the binding constant K_b [40,41] in accordance with the following equation: $K_b \approx (I_0 - I)/(I_0 \times ([FAV] - (I_0 - I)))$.

3. Results and Discussion

3.1. Electrochemical Profiling of Favipiravir on SPE/CNT and SPE/CNT/TiO₂

The rising interest in FAV is ascribed to its efficient suppression of dangerous and even lethal infections caused by numerous viruses, such as hemorrhagic fevers, COVID-19, SARS, MERS, rabies, etc. [8–33], and by its possible efficacy against viruses, which can be transferred to humans from animals and have a high epidemic potential [1,4–6,17,18]. Several drug preparations of FAV have been already developed and registered for clinical use (T-705, Avigan, Favilavir, Avifavir, Areplivir, Coronavir) [5,20–22] and many derivatives and analogs are under development (reviewed in [46]). Clinical usage stimulates FAV research in the field of its side effects and the mechanisms involved therein, and the elaboration of methods of drug control and determination in organs, tissues and the environment.

For quantitative determination of FAV in biological fluids and in pharmaceutical formulations, environmental samples have been collected and several methods have been described, such as UV-Vis spectrophotometry, spectrofluorimetric method, high-performance liquid chromatography (HPLC), and liquid chromatography–tandem mass spectrometry (LC–MS/MS) [47,48]. Electrochemical methods offer great advantages, such as high sensitivity, elaboration of the instrumental equipment with friendly software, quick response rate, usage of low-toxicity reagents, such as aqueous electrolyte buffer solutions, and miniaturization mode for the analysis in a “point-of-care” regimen [49,50].

In our experiments, we used disposable screen-printed electrodes as commercially available transducers, with a relatively low cost, to explore in clinical laboratories their suitability for modifications with different types of nanomaterials [51,52]. Electrochemical profiling of FAV on the screen-printed electrodes modified by single-walled carbon nanotubes (SPE/CNT) and carbon nanotubes with nanosized TiO₂ was studied. Carbon nanomaterials, such as carbon nanotubes and carbon nanotubes with nanosized titanium (IV) oxide TiO₂, significantly improve the sensitivity of electrodes [53–56]. TiO₂ in various forms (nanoparticles, nanotubes, nanoneedles) has properties that make it attractive for the modification of electrodes, such as biocompatibility, specific binding to biomolecules owing to amphoteric chemical nature, optical transparency, large specific surface area for high biomolecule content, and a stimulating effect for electron transfer between the electrode and molecule under investigation [56]. Previously, we employed/applied CNT + titanium (IV) oxide nanoparticles for protein and amino acid immobilization on electrode surface for the fabrication of electrochemical biosensors based on the electrochemical oxidation of amino acids, such as tyrosine, tryptophan, histidine, methionine, and cysteine [42,43]. In

our study, we used this nanomaterial for the electrochemical analysis of FAV. Before the measurements, we used adsorptive accumulation of favipiravir on the electrode surface within 40 min. The electrochemical behavior of FAV was studied in physiologically relevant PBS, with pH 7.4.

Electrochemical analyses were performed using cyclic voltammetry (CV) and the differential pulse voltammetry (DPV) technique. Disposable carbon SPEs modified with CNT (SPE/CNT) and CNT/TiO₂ (SPE/CNT/TiO₂) were used for CV and DPV, respectively. CVs for the 500 μ M FAV in the potential range of 0.6 V \div +1.2 V were analyzed in electrolyte PBS (pH 7.4).

During the anodic scan from 0.6 to +1.2 V, one broad oxidation peak was received at around +0.98 V and +0.96 V for SPE/CNT and SPE/CNT/TiO₂, respectively, while no reduction peak was observed in the reverse cathodic scan (Figure 1a). The peak at E = +0.98 V \div +0.96 V of FAV could reflect the oxidation of the hydroxyl group to the keto group, as was shown earlier [48,49].

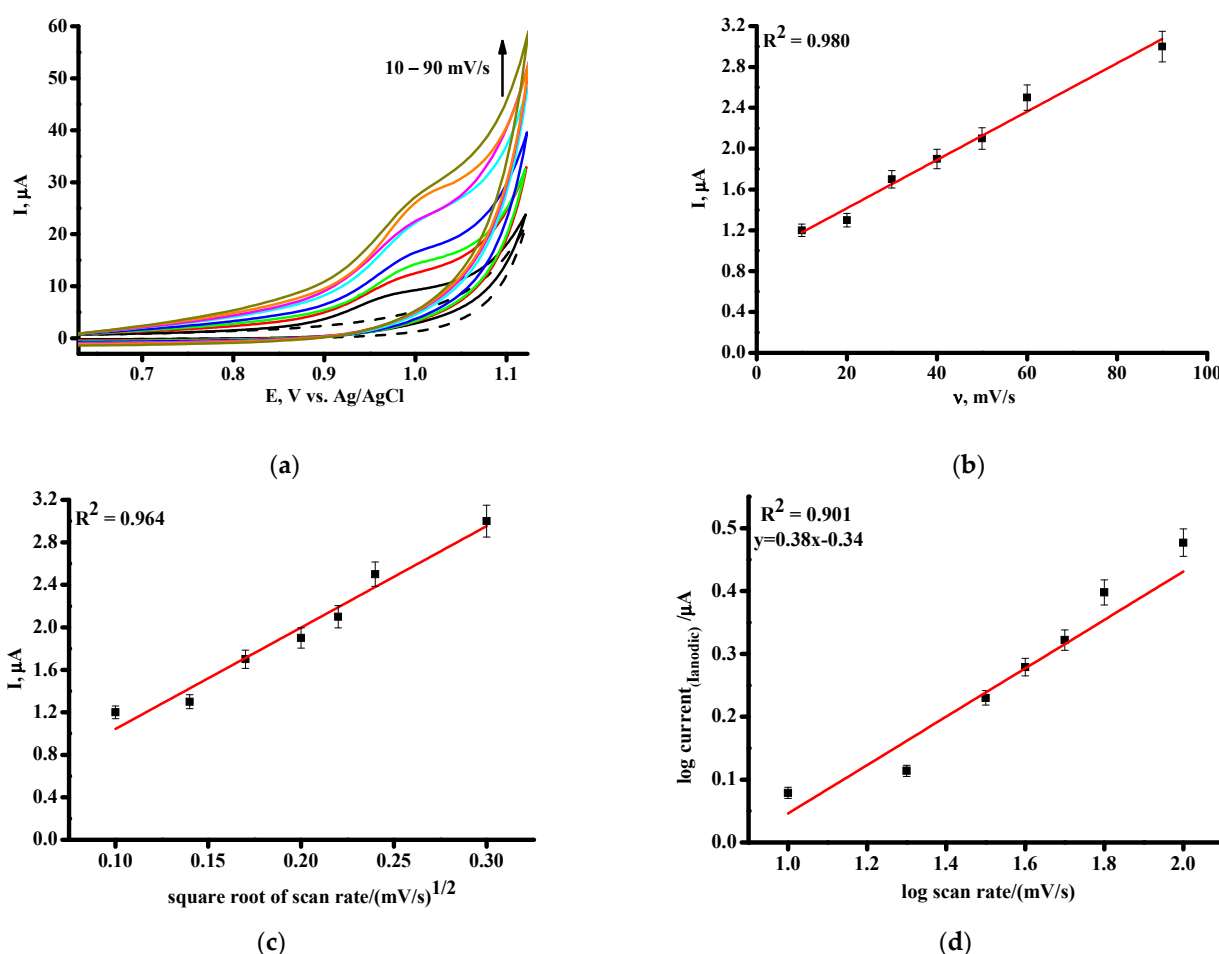


Figure 1. (a) CV of 500 μ M FAV on SPE/CNT at different scan rates from 10 to 90 mV/s, (-), 10 mV/s); (-), 20 mV/s); (-) 40 mV/s); (-) 50 mV/s); (-) 60 mV/s); (-) 70 mV/s); (-) 80 mV/s); (-) 90 mV/s; (b) the linear plot of the oxidation peak current of FAV vs. the scan rate; (c) the linear plot of the oxidation peak current of FAV vs. the square root of the scan rate; (d) Log(I_p) dependence on Log (v).

The oxidation peak potential (E_{pa}) of FAV recorded by cyclic voltammetry shifted towards the positive direction, with the increase in the scan rate as an additional characteristic of an irreversible electrode reaction (Figure 1a) [57–61]. We registered a linear relationship between the oxidation peak current and the scan rate v, and between the oxidation peak current and square root of scan rate v^{1/2} for SPE/CNT (Figure 1b,c) and for SPE/CNT/TiO₂. These experimental dependences indicated that the FAV electro-

chemical oxidation process revealed a mixed mechanism, controlled by both adsorption and diffusion [57–61]. The same properties of the FAV electrochemical oxidation process were also demonstrated while using boron-doped diamond electrodes and carbon electrodes [47,48,62]. The slope of the $\log I_{pa}$ against $\log v$ is 0.38 (Figure 1d); the equation's slope confirmed that the FAV electrochemical oxidation process revealed a mixed mechanism controlled by a mixed diffusion-controlled electrochemical reaction [57–61].

The irreversibility of the oxidation process was also confirmed by means of linear dependence of plot of (E) on logarithmic (v) in accordance with Laviron's theory (Figure S1) [47,48,60–66].

Differential pulse voltammetry (DPV), one of the most sensitive and contemporary electrochemical techniques, possesses high analytical sensitivity, which permits us to register heterocyclic nucleic bases separately for the detailed analysis of intricate drug/DNA interaction mechanism. The DPV of FAV in the potential range of $+0.6 \text{ V} \div +1.2 \text{ V}$ was investigated in electrolyte PBS. The DPV of FAV revealed a single anodic peak at $E = +0.972 \pm 0.003 \text{ V}$ and $E = +0.967 \pm 0.003 \text{ V}$ (Figure 2a) for SPE/CNT and for SPE/CNT/TiO₂, respectively.

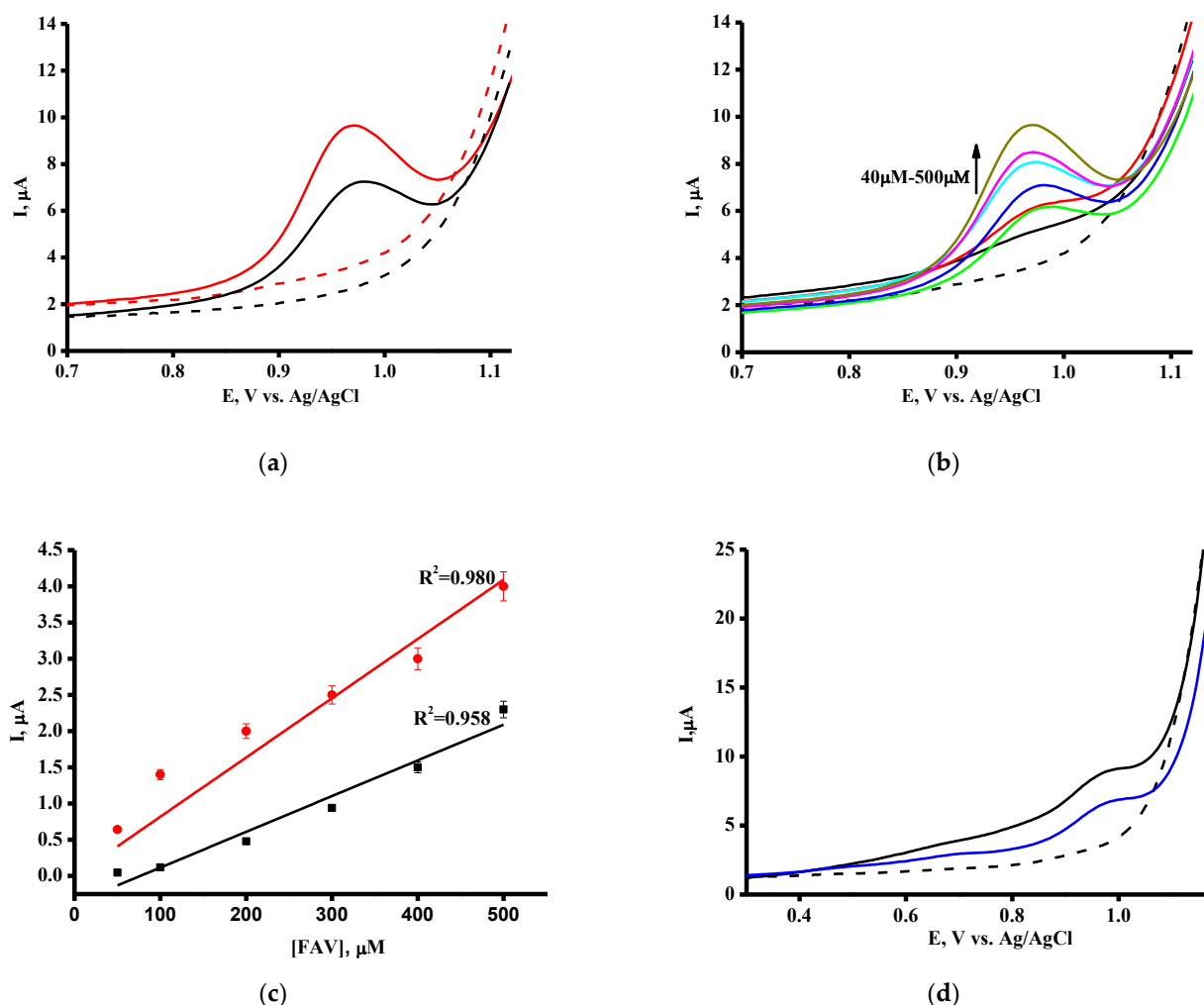


Figure 2. (a) Comparative DPV curves of 500 μM FAV on SPE/CNT (black) and SPE/CNT/TiO₂ (red), (---) and (---) curves corresponded to blank electrodes; (b) DP voltammograms recorded in 0.1 M potassium phosphate electrolyte buffer, pH 7.4 (PBS) with increasing FAV concentration in the range of 50–500 μM (-), 40 μM ; (-) 100 μM ; (-), 150 μM ; (-), 200 μM ; (-) 300 μM ; (-), 400 μM ; (-), 500 μM . Dashed black line represents DPV of SPE/CNT/TiO₂ in PBS. The standard deviation of the DPV response on the SPE/CNT/TiO₂ for three experiments was $\pm 5\%$; (c) DPV peak current versus the concentration of FAV for SPE/CNT (black) and SPE/CNT/TiO₂ (red); (d) DPV of first (-) and second (-) scan of 50 μM FAV on SPE/CNT/TiO₂.

Favipiravir dosing regimens differ for different viral infections. To achieve drug efficacy, medical doses are high and correspond to the micromolar region [46,62]. In our experiments, we used a pharmacologically relevant FAV concentration range from 50 to 500 μM [5,19–22]. For the range of 50–500 μM , the regression equations were $I = (0.0049 \pm 0.0005) [\text{FAV}] - 0.38 \pm 0.10$ and $I = (0.0082 \pm 0.0005) [\text{FAV}] + 0.52 \pm 0.10$ for SPE/CNT or SPE/CNT/TiO₂, respectively (Figure 2b,c). The described method was validated for parameters such as linearity and limits of detection (LOD). Electroanalytical parameters of quantitative FAV analysis with SPE/CNT and SPE/CNT/TiO₂ are presented in Table 1. The sensitivity of SPE/CNT/TiO₂ was approximately twice as high in comparison with SPE/CNT.

Table 1. Electroanalytical parameters of DPV for FAV determination with SPE/CNT and SPE/CNT/TiO₂.

Parameters	SPE/CNT	SPE/CNT/TiO ₂
E_{ox} , V	0.972 ± 0.003	0.967 ± 0.003
Sensitivity, $\mu\text{A}/\mu\text{M}$ (Slope)	0.0049	0.0082
Linear range, μM	50–500	50–500
LOD, μM	60	37
Equation for linear regression ¹	$I_{\text{ox}} = (0.0049 \pm 0.0005) [\text{FAV}] - 0.38 \pm 0.10$	$I_{\text{ox}} = (0.0082 \pm 0.0005) [\text{FAV}] + 0.52 \pm 0.10$
Correlation coefficient, R^2	0.958	0.980

¹ I_{ox} corresponds to the oxidative currents (peak heights) for FAV.

The calculation using Equation (1) and DPV parameters for FAV on SPE/CNT or SPE/CNT/TiO₂ and [67,68] showed that one electron is involved in the oxidation process of this drug [48,62,63,69]:

$$W_{1/2} = 3.52 RT/nF \quad (1)$$

where we used common abbreviations for parameters, as $W_{1/2}$ is the DPV half peak width, R is gas constant, $8.3145 \text{ J K}^{-1} \text{ mol}^{-1}$, T is temperature, in Kelvin, F is Faraday constant $96,485 \text{ C mol}^{-1}$, and n is the number of electrons involved in the oxidation reaction.

The irreversibility of FAV electrochemical oxidation was also confirmed via comparing the first and second scan of DPV, which demonstrated the decline in oxidation current corresponding to the second scan (Figure 2d). On the other hand, the decrease in oxidation peak current might be explained by partial fouling and inactivation of the available electrode surface area [62–67].

Earlier, it was shown that FAV could be analyzed electrochemically using different type of electrodes and modifications [47–50,62,63,69]. FAV can be electro-oxidized using a bimetallic nanocomposite based on gold/silver core–shell nanoparticles with conductive polymer poly (3,4-ethylenedioxythiophene) polystyrene sulfonate and functionalized multi-carbon nanotubes on a glassy carbon electrode. DPV technique and the working potential of 1.25 V with two linear ranges from 0.005 to 0.009 and 0.009 to 1.95 μM with a limit of detection of 0.46 nM ($S/N = 3$) were described [47]. Boron-doped diamond electrodes [48] and screen-printed electrodes modified by means of MnO₂/graphene derivatives [45] were used for the electroanalytical sensing of FAV at the potential of 1.23 V. A comparison of the electroanalytical methods for FAV analysis is given in Table S1.

3.2. Investigation of the Interaction between Favipiravir and dsDNA

Binding models for the interaction between dsDNA and drugs classify them as electrostatic interactions, including binding in minor or major grooves and intercalative binding [36–38,68,70].

Spectroscopic methods are the traditional technique for the investigation of drug/DNA interactions from the pharmacogenomics viewpoint. We analyzed the UV-vis absorption spectra of FAV, dsDNA and the complex of FAV/DNA (Figure 3). FAV shows two absorption peaks at 234 nm and 362 nm. When complex FAV/DNA was formed, a hypochromic

effect (i.e., a decrease in absorbance) at 257 nm was recorded together with a slight hypsochromic blue shift. As can be seen from Figure 3, FAV, FAV/DNA complex and DNA have absorption spectra with close maximum wavelengths. Therefore, the explanation of the mechanism of drug/DNA interaction is ambiguous. However, based on the hypochromic effect, it is possible to propose that FAV interacts with DNA in accordance with the intercalative mechanism [69].

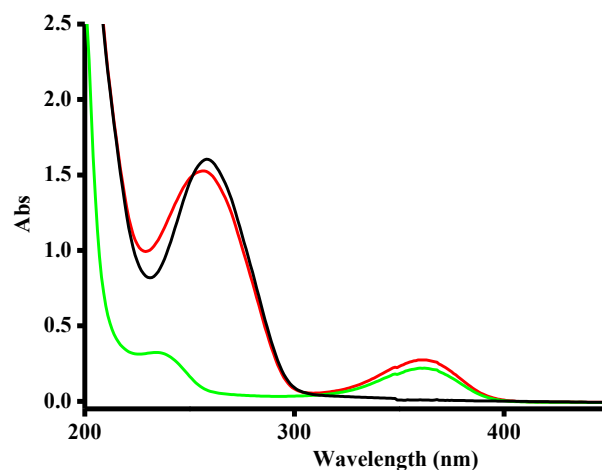


Figure 3. Absorption spectra in presence of 0.075 mg/mL dsDNA (black), 25 μ M FAV (green), and FAV/dsDNA complex (red) in PBS.

The electrochemical technique was used for the investigation of the FAV/dsDNA interaction mechanism as a sensitive and robust technology. Earlier, we showed that electrochemical oxidation of dsDNA was successfully achieved on SPE/CNT after dsDNA immobilization by physical entrapment/absorption on the surface of the modified electrodes. Modification of SPEs with CNT stabilized with carboxymethylcellulose (SPE/CNT) allowed the registering of electrochemical oxidation of guanine, adenine and thymine in the immobilized dsDNA [40,41,71]. Adding nanosized titanium (IV) oxide TiO₂ improved the sensitivity of electrodes for the registration of dsDNA (Figure 4a,b), as in the case of protein registration [43]. Based on this data, we used SPE/CNT/TiO₂ for the investigation of interaction between FAV and dsDNA. We carried out electrochemical measurements with the DPV method. DPV was chosen as a sensitive and informative technique for drug/DNA assay. The main advantage of DPV is also a significant decline in the contribution of capacitive current in comparison with faradaic current.

DPV of the first (black line) and second (red line) scan of dsDNA (1.5 mg/mL) on SPE/CNT/TiO₂ demonstrated the irreversible nature of the electrochemical process and fouling of the electrode by means of DNA or FAV oxidation products (Figure 4c) [71,72]. Based on this observation, we used SPEs only for single measurements. This regimen is typical for the irreversible electrochemical process [40,41,73].

DNA carries genetic information required for the synthesis of proteins. Apart from this role of DNA, different types of DNA or RNA molecules may be present in normal and pathological cells and fluids in human body, such as circulating tumor DNA (ctDNA), microRNA, therapeutic nucleic acids and cell free DNA (cfDNA). These types of DNA or RNA possess diagnostic relevance as specific markers of diseases and play a role in organism defense at the transcription/translation regulation level [72,74–77]. The detection of DNA/drug complex formation and study of the mode of interactions are the main points of pharmacogenomics [36,78–83].

FAV itself demonstrated a DPV oxidation signal at around +0.96 \div +1 V, in the region of non-overlapping potentials with nucleobases oxidation potentials. Therefore, the investigation of binding of FAV with dsDNA via electrochemical methods was more effective in comparison with the spectrophotometric technique by means of the observation of changes

in peak current intensity of guanine, adenine and thymine of DNA in the presence of FAV (Figure 5a).

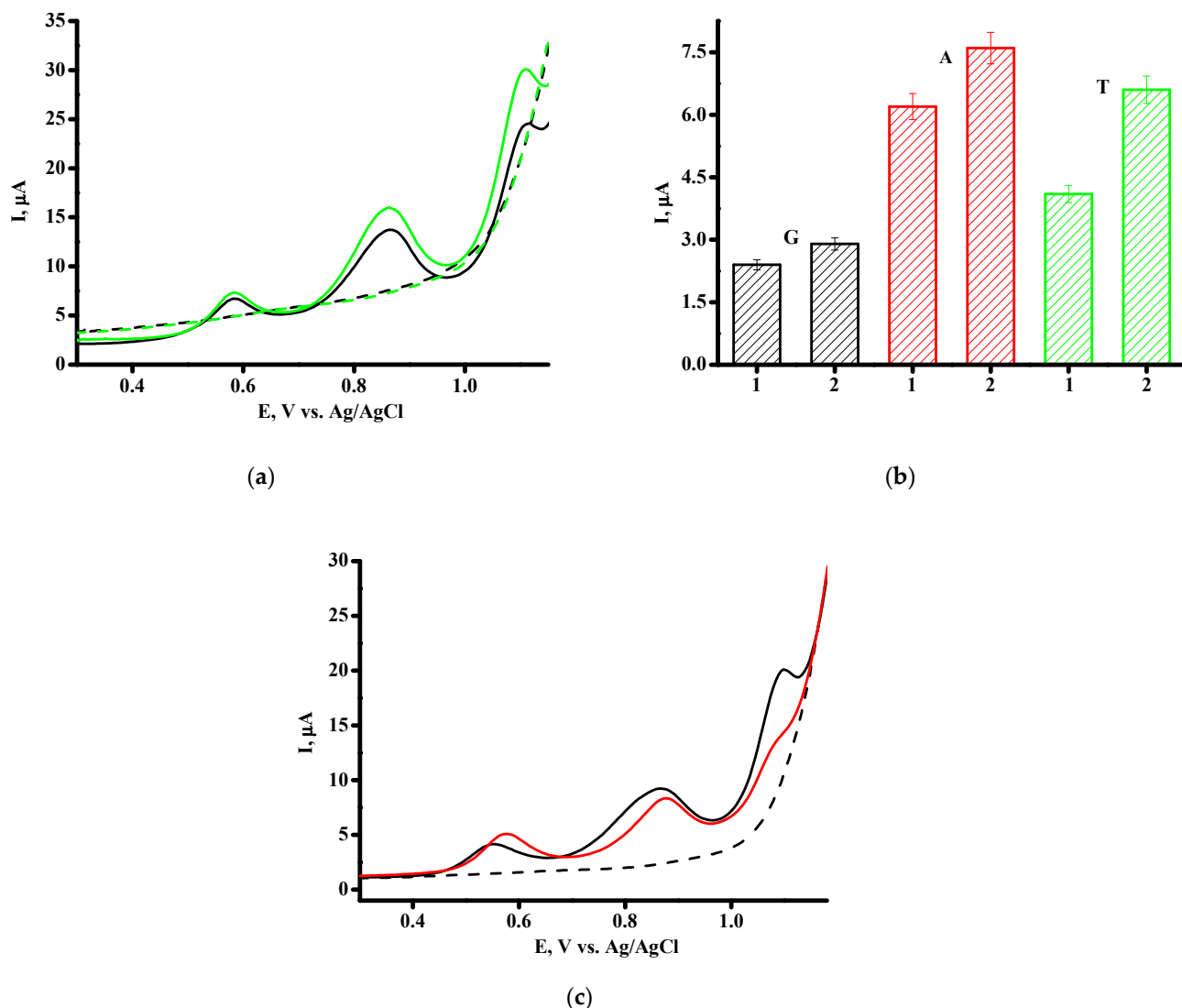


Figure 4. (a) DPV of dsDNA (1.5 mg/mL) on SPE/CNT (black line) and SPE/CNT/TiO₂ (green line), blank SPE/CNT (---) and SPE/CNT/TiO₂ (---); (b) histogram of oxidation peak current for dsDNA (1.5 mg/mL) for SPE/CNT (1) and SPE/CNT/TiO₂ (2); (c) DPV of first (black line) and second scan (red line) of dsDNA (1.5 mg/mL) on SPE/CNT/TiO₂.

Electrochemical analysis of dsDNA based on direct electrochemical oxidation of guanine, adenine and thymine residues [82] was used. This technique was applied for the analysis of the interactions of FAV with DNA. In our designed experimental approach, we used the increased concentration of FAV in the range of 50–500 μM and registered the DPV peak current intensity of G, A and T oxidation of a constant concentration of dsDNA (1.5 mg/mL) immobilized on single-use SPE/CNT/TiO₂. It is a well-known viewpoint that the positive shift of the oxidation of heterocyclic bases peak potentials is typical for the intercalative hydrophobic mode of drugs during binding to DNA. In contrast, the negative shift is representative of the binding modes such as electrostatic interaction or groove binding [35–38,80,83]. In order to determine the optimum time for FAV/dsDNA complex formation, we compare the intensities of nucleic bases' oxidation signals after the interaction of dsDNA with 500 μM in time intervals of 5 and 40 min. The main question of complex formation in a non-covalent system with a reversible equilibrium is to find the balance between complex formation and complex dissociation. We have shown that 40 min

interaction time is optimum for an FAV/dsDNA complex (Figure 5a). For this reason, we incubated the complex for 40 min before electrochemical measuring.

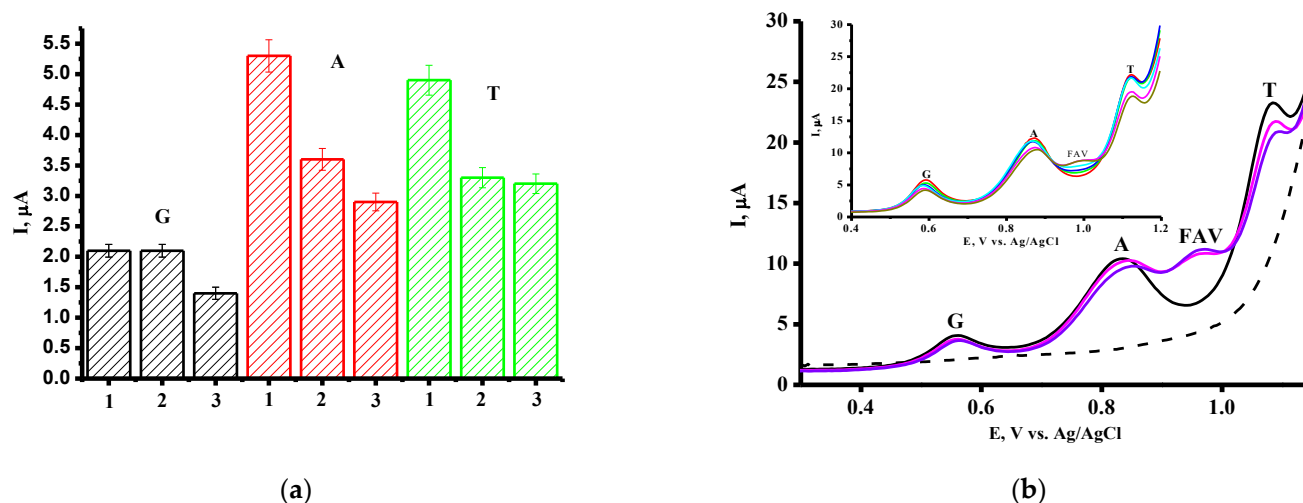


Figure 5. (a) The average guanine, adenine and thymine signals after interaction with 500 μM FAV at 0 min (1), 5 min (2) and 40 min (3); (b) DPV of dsDNA (1.5 mg/mL) on SPE/CNT/TiO₂ (black line), blank SPE/CNT/TiO₂ (---) and FAV/dsDNA complex with 400 μM FAV concentration (-), 500 μM FAV concentration (-). Inset: DP voltammograms of dsDNA in the presence of FAV in the concentration range of 50–500 μM (from (-, 50 μM) to (-, 500 μM)).

The adequacy of the proposed approach was evaluated by experiments in which the dsDNA sensor was incubated in phosphate buffer pH 7.4 without adding FAV. No changes in G, A or T oxidative peak current intensities were observed. In contrast, the interaction of dsDNA with FAV is accompanied by a decrease in the peak current intensities of G, A and T heterocyclic bases (Figure 5b). The influence of FAV is accompanied by a shift of the oxidation potentials of the heterocyclic bases of G, A and T in the anodic direction, registered as 4 ± 2 mV, 10 ± 2 mV and 5 ± 2 mV, respectively. The most pronounced shift was registered for adenine oxidation. Based on this experimental data, it is possible to assume that FAV interacts more intensively with adenine than with guanine or thymine. Positive shifts, observed for registered heterocyclic bases, corresponded to the intercalative mode of drug/DNA interaction mechanisms, as was confirmed during the study of numerous examples [48–52].

Investigation of the mechanism of the FAV inhibition mode revealed that FAV can form FAV:G and FAV:A pairs with pyrimidine-like analog behavior [29]. To estimate the mode of interaction, the binding constants for the complex FAV/dsDNA were calculated based on the values of the oxidation current of nucleobases before and after the interaction of DNA with the drug, in accordance with an earlier-published approach for the determination of this parameter [54,72] (Figure S2). Intercalation-based interactions are characterized by high K_b values, usually 10^4 – 10^6 M^{-1} , while lower K_b values imply a rather weaker interaction, such as groove or electrostatic interactions [36,38,78–80]. The structure of FAV permits the formation of two hydrogen bonds with adenine residue. The Watson–Crick hydrogen bonding in a canonical G–C pair requires the formation of three bonds; however, FAV cannot constitute exactly three bonds. Based on this speculation, it is possible to explain the most intensive interaction of FAV with the adenine nucleobase [29].

The values of K_b confirmed the intercalative mode of FAV/DNA interaction (Table 2). The changes in Gibbs free energy, ΔG , were found to be negative, and confirmed that FAV/DNA interaction was spontaneous and energetically favorable (Table 2).

Table 2. Values of FAV/dsDNA binding constants (K_b) and the Gibbs free energy (ΔG).

FAV/dsDNA	K_b, M^{-1}	$\Delta G = -RT \ln K_b, kJ/mol$
Based on G oxidation signals	0.24×10^4	-18.96
Based on A oxidation signals	1.03×10^4	-22.51
Based on T oxidation signals	0.20×10^4	-18.52

The influence of FAV was also represented as the DNA-mediated electrochemical coefficient of toxicity using Equation (2):

$$S = (S_s/S_b) \times 100\% \quad (2)$$

where S_b and S_s are nucleobase oxidation signals before and after interaction of the FAV with dsDNA, respectively [40,41,84]. We used this criterion such that if a drug does not have a toxic effect, S is higher than 85%; it has a moderate toxic effect if the S parameter is between 50 and 85%, and has a toxic effect if S is below 50% [83]. FAV manifested a toxic effect only at a 500 μM concentration (Figure 6a–c).

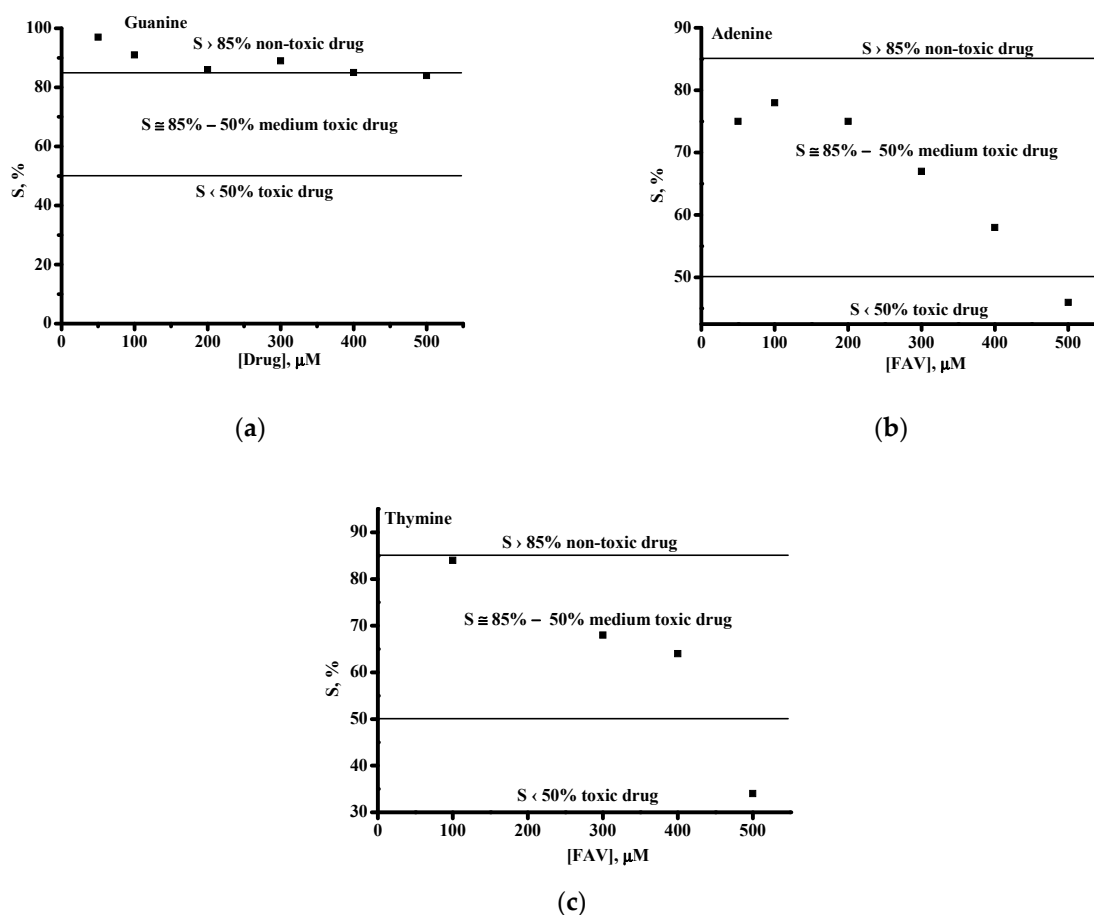


Figure 6. DNA-mediated electrochemical coefficient of toxic effect, S (%), of FAV in the concentration range of 50–500 μM on the signals of electrooxidation of guanine (a), adenine (b) and thymine (c) heterocyclic bases.

Double-stranded DNA from calf thymus (ctDNA) was also used as a molecular bio model for the investigation of the interaction with FAV. A total of 2 μL of samples was allowed to rest for 10 min at +37 $^{\circ}C$ on the surface of the SPE/CNT/TiO₂ electrodes before measurements. A horizontal measurement regimen in a 60 μL drop of PBS placed onto the SPE to cover the surface of all three electrodes was used for all measurements. As can be seen from Figure 7, the SW voltammogram of ctDNA revealed only one broad peak,

centered at a potential of $+0.84 \pm 0.01$ V, and under complex formation, the FAV/ctDNA peak potential shifted by 0.03 V to the more positive direction (0.87 ± 0.01 V), confirming the intercalative mode of interaction with FAV. In comparison with low-molecular-weight dsDNA from salmon sperm, demonstrating three clear peaks, calf thymus DNA exhibited only one peak due to the more compact structure of the DNA molecule [82–84]. Investigation of the interaction of the drug with dsDNA permits us to register G, A and T separately and to register the electrochemical response of each base upon drug intake.

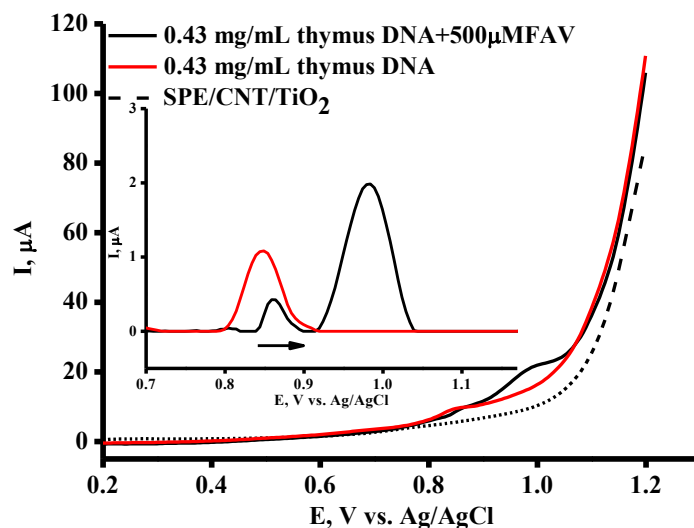


Figure 7. SW voltammograms of 0.43 mg/mL ctDNA (-) and 0.43 mg/mL ctDNA + 500 μ M FAV (-); SPE/CNT (---). Inset: the current intensities of the base line corrected SWV peaks for electrochemical oxidation of the ctDNA (-) and for complex ctDNA+500 μ M FAV (-).

Adverse effects of FAV, such as genotoxicity and oxidative stress, were investigated at the molecular level in cell models [23]. When H9c2 cardiomyoblasts or CCD-1079Sk skin fibroblasts were treated with FAV for 24 h, significant DNA damage was registered with Comet assay at a 400 μ M FAV concentration, confirming the genotoxic effects of FAV [23]. In our experiments, we incubated dsDNA with FAV (50–500 μ M) for 24 h and observed an increase in the oxidative peak current of the heterocyclic bases with negative shifts of oxidation potentials, especially pronounced for A and T residue (registered as 3 ± 1 mV (G), 13 ± 2 mV (A) and 15 ± 2 mV (T) (Figure 8).

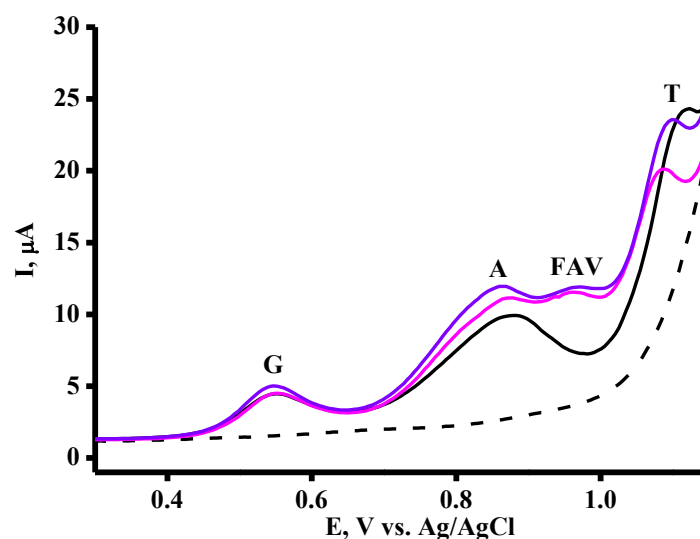


Figure 8. DPV of dsDNA (1.5 mg/mL) on SPE/CNT/TiO₂ (black line), blank SPE/CNT/TiO₂ (---) and FAV/dsDNA complex with 400 μ M (-) and 500 μ M FAV concentrations (-) after 24 h incubation.

The increase in current may reflect the damage to DNA during prolonged incubation with FAV. The negative shift of oxidation potential during 24 h FAV treatment with DNA reflects the transition of the binding mode of DNA/drug interaction from intercalative to electrostatic attraction-assisted groove-binding interactions. Based on the chemical structure of FAV as 6-fluoro-3-hydroxypyrazine-2-carboxamide (Scheme 1), it is possible to assume that this drug not only intercalates into DNA molecule but also forms hydrogen and ionic bonds through NH_2 - and HO- groups as a secondary process of the prolonged incubation of FAV with dsDNA.

4. Conclusions

Favipiravir (FAV) is an effective antiviral medication for curing COVID-19 and other infections caused by RNA viruses. However, the interaction of this drug with dsDNA had not been studied earlier. The next focus of our experiments will be the investigation of the pharmacogenomic properties of favipiravir in the process of drug/DNA complex formation. Electrochemistry, as a modern and sensitive platform for the analysis of drug/DNA interactions, possesses remarkable advantages, such as miniaturization, high sensitivity and broad potential window permitting registration of the drug itself and the DNA response as oxidation signals of nucleic bases [35–38,41,42,81,83,84]. This study utilizes single-use electrodes (SPE/CNT/TiO₂/DNA) as sensing elements for the investigation of the antiviral drug favipiravir's interaction with dsDNA. Voltammetric detection of DNA before and after the concentration-dependent drug complex formation permits the calculation of the binding constants K_b of FAV/dsDNA complexes for guanine, adenine and thymine. The qualitative characteristics of FAV/dsDNA interaction, such as the DNA-mediated electrochemical coefficient of toxicity, were also determined. FAV revealed non-toxic or moderate toxic effects in the concentration range of 50–400 μM . Based on the values of the equilibrium constant K_b as 10^4M^{-1} and shifts of the oxidation potentials of heterocyclic nucleobases to the anodic direction (4–10 mV), we concluded that FAV interacted with DNA via an intercalative mode. We registered the most pronounced effect for adenine in comparison with guanine and thymine residues. The changes in Gibbs free energy ΔG were calculated as negative values, confirming the spontaneous process of complex formation. Favipiravir's adverse effect during 24 h incubation with dsDNA was shown. The increase in the oxidation current of DNA could reflect the damage to DNA during the prolonged incubation with FAV.

The novelty of our study is the elucidation of the structural changes in DNA after interaction with the antiviral drug favipiravir using a DNA detection approach based on an electrochemical DNA biosensor. In our investigation, we used a new composite material for electrode modification, carbon nanotubes with titanium oxide nanoparticles, allowing us to improve the sensitivity of the analysis. For registration of binding events as models of pharmacogenomics, we used dsDNA from fish sperm and calf thymus DNA. We discovered that favipiravir showed a mechanism that is more complicated during prolonged incubation with DNA. Monitoring of drug/DNA interactions by means of an electrochemical technique has great promise and may help in the development of new pharmaceuticals.

Supplementary Materials: The following supporting information can be downloaded at: <https://www.mdpi.com/article/10.3390/pharmaceutics16040503/s1>, Figure S1: The relationship between E_{pa} vs. $\ln v$ at the surface of on SPE/CNT; Figure S2: Linear plots for $1/(I_0 - I)$ depending on $1/[\text{drug}]$: (a) FAV/dsDNA (for guanine signals); equation for linear fit: $y = 718x + 1.75 \cdot 10^6$, $R^2 = 0.899$, $K_b = 0.24 \cdot 10^4 \text{M}^{-1}$; (b) FAV/dsDNA (for adenine signals); equation for linear fit: $y = 221x + 2.29$; $R^2 = 0.917$, $K_b = 1.03 \cdot 10^4 \text{M}^{-1}$; (c) FAV/dsDNA (for thymine signals); equation for linear fit: $y = 120.45x + 241154$, $R^2 = 0.927$, $K_b = 0.20 \cdot 10^4\text{M}^{-1}$; Table S1: Electrochemical FAV detection based on electro oxidation.

Author Contributions: V.V.S. and E.F.K. contributed to the conception and design of the study; T.V.B. and L.E.A. performed the electrochemical experiments, V.V.S. and L.E.A. performed the theoretical

calculations; V.V.S. wrote the first draft of the manuscript; E.F.K., A.A.C. and L.E.A. wrote sections of the manuscript. All authors contributed to manuscript revision and read and approved the submitted version. All authors have read and agreed to the published version of the manuscript.

Funding: This work was financed by the Ministry of Science and Higher Education of the Russian Federation within the framework of state support for the creation and development of World-Class Research Centers “Digital biodesign and Personalized Healthcare” No. 075-15-2022-305.

Institutional Review Board Statement: Not applicable.

Informed Consent Statement: Not applicable.

Data Availability Statement: The data presented in this study are available in this article (and Supplementary Materials).

Conflicts of Interest: The authors declare no conflicts of interest.

References

1. Madelain, V.; Mentré, F.; Baize, S.; Anglaret, X.; Laouénan, C.; Oestereich, L.; Nguyen, T.H.T.; Malvy, D.; Piorowski, G.; Graw, F.; et al. Modeling favipiravir antiviral efficacy against emerging viruses: From animal studies to clinical trials. *CPT Pharmacomet. Syst. Pharmacol.* **2020**, *9*, 258–271. [[CrossRef](#)] [[PubMed](#)]
2. Furuta, Y.; Takahashi, K.; Fukuda, Y.; Kuno, M.; Kamiyama, T.; Kozaki, K.; Nomura, N.; Egawa, H.; Minami, S.; Watanabe, Y.; et al. In vitro and in vivo activities of anti-influenza virus compound T-705. *Antimicrob. Agents Chemother.* **2002**, *46*, 977–981. [[CrossRef](#)] [[PubMed](#)]
3. Furuta, Y.; Takahashi, K.; Kuno-Maekawa, M.; Sangawa, H.; Uehara, S.; Kozaki, K.; Nomura, N.; Egawa, H.; Shiraki, K. Mechanism of action of T-705 against influenza virus. *Antimicrob. Agents Chemother.* **2005**, *49*, 981–986. [[CrossRef](#)] [[PubMed](#)]
4. Kiso, M.; Takahashi, K.; Sakai-Tagawa, Y.; Shinya, K.; Sakabe, S.; Le, Q.M.; Ozawa, M.; Furuta, Y.; Kawaoka, Y. T-705 (favipiravir) activity against lethal H5N1 influenza A viruses. *Proc. Natl. Acad. Sci. USA* **2010**, *107*, 882–887. [[CrossRef](#)] [[PubMed](#)]
5. *Pharmaceuticals and Medical Devices Agency, Report on the Deliberation Results—Avigan*; Evaluation and Licensing Division, Pharmaceutical and Food Safety Bureau: Tokyo, Japan, 2011. Available online: www.pmda.go.jp/files/000210319.pdf (accessed on 30 October 2023).
6. Fang, Q.Q.; Huang, W.J.; Li, X.Y.; Cheng, Y.H.; Tan, M.J.; Liu, J.; Wei, H.J.; Meng, Y.; Wang, D.Y. Effectiveness of favipiravir (T-705) against wild-type and oseltamivir-resistant influenza B virus in mice. *Virology* **2020**, *545*, 1–9. [[CrossRef](#)] [[PubMed](#)]
7. Pires de Mello, C.P.; Tao, X.; Kim, T.H.; Bulitta, J.B.; Rodriguez, J.L.; Pomeroy, J.J.; Brown, A.N. Zika virus replication is substantially inhibited by novel favipiravir and interferon alpha combination regimens. *Antimicrob. Agents Chemother.* **2017**, *62*, e01983-17. [[CrossRef](#)] [[PubMed](#)]
8. Madelain, V.; Guedj, J.; Mentré, F.; Nguyen, T.H.; Jacquot, F.; Oestereich, L.; Kadota, T.; Yamada, K.; Taburet, A.M.; de Lamballerie, X.; et al. Favipiravir pharmacokinetics in nonhuman primates and insights for future efficacy studies of hemorrhagic fever viruses. *Antimicrob. Agents Chemother.* **2016**, *61*, e01305-16. [[CrossRef](#)] [[PubMed](#)]
9. Escribano-Romero, E.; Jiménez de Oya, N.; Domingo, E.; Saiz, J.C. Extinction of West Nile virus by favipiravir through lethal mutagenesis. *Antimicrob. Agents Chemother.* **2017**, *61*, e01400-17. [[CrossRef](#)] [[PubMed](#)]
10. Borrego, B.; de Ávila, A.I.; Domingo, E.; Brun, A. Lethal mutagenesis of Rift Valley Fever Virus Induced by Favipiravir. *Antimicrob. Agents Chemother.* **2019**, *63*, e00669-19. [[CrossRef](#)] [[PubMed](#)]
11. Oestereich, L.; Rieger, T.; Neumann, M.; Bernreuther, C.; Lehmann, M.; Krasemann, S.; Wurr, S.; Emmerich, P.; de Lamballerie, X.; Ölschläger, S.; et al. Evaluation of antiviral efficacy of ribavirin, arbidol, and T-705 (favipiravir) in a mouse model for Crimean-Congo hemorrhagic fever. *PLoS Negl. Trop. Dis.* **2014**, *8*, 2804. [[CrossRef](#)] [[PubMed](#)]
12. Mendenhall, M.; Russell, A.; Smeeth, D.F.; Hall, J.O.; Skirpstunas, R.; Furuta, Y.; Gowen, B.B. Effective oral favipiravir (T-705) therapy initiated after the onset of clinical disease in a model of arenavirus hemorrhagic fever. *PLoS Negl. Trop. Dis.* **2011**, *5*, e1342. [[CrossRef](#)] [[PubMed](#)]
13. Smyk, J.M.; Majewska, A. Favipiravir in the battle with respiratory viruses. *Mini Rev. Med. Chem.* **2022**, *22*, 2224–2236. [[CrossRef](#)] [[PubMed](#)]
14. Jochmans, D.; van Nieuwkoop, S.; Smits, S.L.; Neyts, J.; Fouchier, R.A.; van den Hoogen, B.G. Antiviral activity of favipiravir (T-705) against a broad range of paramyxoviruses in vitro and against human metapneumovirus in hamsters. *Antimicrob. Agents Chemother.* **2016**, *60*, 4620–4629. [[CrossRef](#)] [[PubMed](#)]
15. Kerber, R.; Lorenz, E.; Duraffour, S.; Sissoko, D.; Rudolf, M.; Jaeger, A.; Cisse, S.D.; Camara, A.M.; Miranda, O.; Castro, C.M.; et al. Laboratory findings, compassionate use of favipiravir, and outcome in patients with Ebola virus disease, Guinea, 2015-A Retrospective observational study. *J. Infect. Dis.* **2019**, *220*, 195–202. [[CrossRef](#)] [[PubMed](#)]
16. Ren, M.; Zhou, Y.; Tu, T.; Jiang, D.; Pang, M.; Li, Y.; Luo, Y.; Yao, X.; Yang, Z.; Wang, Y. RVG peptide-functionalized favipiravir nanoparticle delivery system facilitates antiviral therapy of neurotropic virus infection in a mouse model. *Int. J. Mol. Sci.* **2023**, *24*, 5851. [[CrossRef](#)] [[PubMed](#)]

17. Takashita, E.; Morita, H.; Nagata, S.; Shirakura, M.; Fujisaki, S.; Miura, H.; Takayama, I.; Arita, T.; Suzuki, Y.; Yamaoka, M.; et al. Influenza Virus Surveillance Group of Japan. Antiviral susceptibilities of avian influenza A(H5), A(H7), and A(H9) viruses isolated in Japan. *Jpn. J. Infect. Dis.* **2022**, *75*, 398–402. [[CrossRef](#)] [[PubMed](#)]
18. Zaraket, H.; Saito, R. Japanese surveillance systems and treatment for influenza. *Curr. Treat. Options Infect. Dis.* **2016**, *8*, 311–328. [[CrossRef](#)] [[PubMed](#)]
19. Chen, C.; Zhang, Y.; Huang, J.; Yin, P.; Cheng, Z.; Wu, J.; Chen, S.; Zhang, Y.; Chen, B.; Lu, M.; et al. Favipiravir versus arbidol for clinical recovery rate in moderate and severe adult COVID-19 patients: A prospective, multicenter, open-label, randomized controlled clinical trial. *Front. Pharmacol.* **2021**, *12*, 683296. [[CrossRef](#)] [[PubMed](#)]
20. Ivashchenko, A.A.; Dmitriev, K.A.; Vostokova, N.V.; Azarova, V.N.; Blinow, A.A.; Egorova, A.N.; Gordeev, I.G.; Ilin, A.P.; Karapetian, R.N.; Kravchenko, D.V.; et al. AVIFAVIR for treatment of patients with moderate coronavirus disease 2019 (COVID-19): Interim results of a phase II/III multicenter randomized clinical trial. *Clin. Infect. Dis.* **2021**, *73*, 531–534. [[CrossRef](#)] [[PubMed](#)]
21. Ruzhentsova, T.A.; Oseshnyuk, R.A.; Soluyanova, T.N.; Dmitrikova, E.P.; Mustafaev, D.M.; Pokrovskiy, K.A.; Markova, T.N.; Rusanova, M.G.; Kostina, N.E.; Agafina, A.S.; et al. Phase 3 trial of coronavir (favipiravir) in patients with mild to moderate COVID-19. *Am. J. Transl. Res.* **2021**, *13*, 12575–12587. [[CrossRef](#)] [[PubMed](#)]
22. Hung, D.T.; Ghula, S.; Aziz, J.M.A.; Makram, A.M.; Tawfik, G.M.; Abozaid, A.A.; Pancharatnam, R.A.; Ibrahim, A.M.; Shabouk, M.B.; Turnage, M.; et al. The efficacy and adverse effects of favipiravir on patients with COVID-19: A systematic review and meta-analysis of published clinical trials and observational studies. *Int. J. Infect. Dis.* **2022**, *120*, 217–227. [[CrossRef](#)] [[PubMed](#)]
23. Gunaydin-Akyildiz, A.; Aksoy, N.; Boran, T.; Ilhan, E.N.; Ozhan, G. Favipiravir induces oxidative stress and genotoxicity in cardiac and skin cells. *Toxicol. Lett.* **2022**, *371*, 9–16. [[CrossRef](#)] [[PubMed](#)]
24. Almutairi, A.O.; El-Readi, M.Z.; Althubiti, M.; Alhindi, Y.Z.; Ayoub, N.; Alzahrani, A.R.; Al-Ghamdi, S.S.; Eid, S.Y. Liver injury in favipiravir-treated COVID-19 patients: Retrospective single-center cohort study. *Trop. Med. Infect. Dis.* **2023**, *8*, 129. [[CrossRef](#)] [[PubMed](#)]
25. Jin, Z.; Smith, L.K.; Rajwanshi, V.K.; Kim, B.; Deval, J. The ambiguous base-pairing and high substrate efficiency of T-705 (Favipiravir) Ribofuranosyl 5'-triphosphate towards influenza A virus polymerase. *PLoS ONE* **2013**, *8*, e68347. [[CrossRef](#)] [[PubMed](#)]
26. Naesens, L.; Guddat, L.W.; Keough, D.T.; van Kuilenburg, A.B.P.; Meijer, J.; Voorde, J.V.; Balzarini, J. Role of human hypoxanthine guanine phosphoribosyltransferase in activation of the antiviral agent T-705 (favipiravir). *Mol. Pharmacol.* **2013**, *84*, 615–629. [[CrossRef](#)] [[PubMed](#)]
27. Huchting, J.; Vanderlinden, E.; Winkler, M.; Nasser, H.; Naesens, L.; Meier, C. Prodrugs of the phosphoribosylated forms of hydroxypyrazinecarboxamide pseudobase T-705 and its de-fluoro analogue T-1105 as potent influenza virus inhibitors. *J. Med. Chem.* **2018**, *61*, 6193–6210. [[CrossRef](#)] [[PubMed](#)]
28. Baranovich, T.; Wong, S.-S.; Armstrong, J.; Marjuki, H.; Webby, R.J.; Webster, R.G.; Govorkova, E.A. T-705 (favipiravir) induces lethal mutagenesis in influenza A H1N1 viruses in vitro. *J. Virol.* **2013**, *87*, 3741–3751. [[CrossRef](#)] [[PubMed](#)]
29. Jena, N.R. Role of different tautomers in the base-pairing abilities of some of the vital antiviral drugs used against COVID-19. *Phys. Chem. Chem. Phys.* **2022**, *22*, 28115–28122. [[CrossRef](#)] [[PubMed](#)]
30. de Ávila, A.I.; Gallego, I.; Soria, M.E.; Gregori, J.; Quer, J.; Esteban, J.I.; Rice, C.M.; Domingo, E.; Perales, C. Lethal mutagenesis of hepatitis C virus induced by favipiravir. *PLoS ONE* **2016**, *11*, e0164691. [[CrossRef](#)] [[PubMed](#)]
31. Vanderlinden, E.; Vrancken, B.; Van Houdt, J.; Rajwanshi, V.K.; Gillemot, S.; Andrei, G.; Lemey, P.; Naesens, L. Distinct effects of T-705 (favipiravir) and ribavirin on influenza virus replication and viral RNA synthesis. *Antimicrob. Agents Chemother.* **2016**, *60*, 6679–6691. [[CrossRef](#)]
32. Wang, Y.; Yuan, C.; Xu, X.; Chong, T.H.; Zhang, L.; Cheung, P.P.-H.; Huang, X. The mechanism of action of T-705 as a unique delayed chain terminator on influenza viral polymerase transcription. *Biophys. Chem.* **2021**, *277*, 106652. [[CrossRef](#)] [[PubMed](#)]
33. Huchting, J.; Vanderlinden, E.; Van Berwaer, R.; Meier, C.; Naesens, L. Cell line-dependent activation and antiviral activity of T-1105, the non-fluorinated analogue of T-705 (favipiravir). *Antivir. Res.* **2019**, *167*, 1–5. [[CrossRef](#)] [[PubMed](#)]
34. Sumitha, M.S.; Xavier, T.S. Recent advances in electrochemical biosensors—A brief review. *Hybrid Adv.* **2023**, *2*, 100023. [[CrossRef](#)]
35. Kurbanoglu, S.; Dogan-Topal, B.; Rodriguez, E.P.; Bozal-Palabiyik, B.; Ozkan, S.A.; Uslu, B. Advances in electrochemical DNA biosensors and their interaction mechanism with pharmaceuticals. *J. Electroanal. Chem.* **2016**, *775*, 8–26. [[CrossRef](#)]
36. Hasanzadeh, M.; Shadjou, N. Pharmacogenomic study using bio- and nanobioelectrochemistry: Drug–DNA interaction. *Mater. Sci. Eng. C Mater. Biol. Appl.* **2016**, *61*, 1002–1017. [[CrossRef](#)] [[PubMed](#)]
37. Ramotowska, S.; Ciesielska, A.; Makowski, M. What can electrochemical methods offer in determining DNA–drug interactions? *Molecules* **2021**, *26*, 3478. [[CrossRef](#)] [[PubMed](#)]
38. Rehman, S.; Sarwar, T.; Husain, M.; Ishqi, H.; Tabish, M. Studying non-covalent drug–DNA interactions. *Arch. Biochem. Biophys.* **2015**, *576*, 49–60. [[CrossRef](#)] [[PubMed](#)]
39. Held, P.G. *Nucleic Acid Purity Assessment Using A260/A280 Ratios*; BioTek Instruments Incorporation: Winooski, VT, USA, 2006; pp. 1–5.
40. Shumyantseva, V.V.; Bulko, T.V.; Agafonova, L.E.; Pronina, V.V.; Kostyukova, L.V. Comparative analysis of the interaction between the antiviral drug umifenovir and umifenovir encapsulated in phospholipids micelles (nanosome/umifenovir) with dsDNA as a model for pharmacogenomic analysis by electrochemical methods. *Processes* **2023**, *11*, 922. [[CrossRef](#)]

41. Pronina, V.V.; Kostryukova, L.V.; Bulko, T.V.; Shumyantseva, V.V. Interaction of doxorubicin embedded into phospholipid nanoparticles and targeted peptide-modified phospholipid nanoparticles with DNA. *Molecules* **2023**, *28*, 5317. [[CrossRef](#)] [[PubMed](#)]
42. Shumyantseva, V.V.; Bulko, T.V.; Kuzikov, A.V.; Khan, R.; Archakov, A.I. Development of methods for functionalization of screen-printed electrodes with biocompatible organic-inorganic hybrid nanocomposites for biosensing applications. *Biochem. (Mos.) Sup. Ser. B Biomed. Chem.* **2014**, *8*, 237–242. [[CrossRef](#)]
43. Shumyantseva, V.V.; Bulko, T.V.; Kuzikov, A.V.; Masamrekh, R.; Archakov, A.I. Analysis of L-tyrosine based on electrocatalytic oxidative reactions via screen-printed electrodes modified with multi-walled carbon nanotubes and nanosized titanium oxide (TiO₂). *Amino Acids* **2018**, *50*, 823–829. [[CrossRef](#)] [[PubMed](#)]
44. Miller, J.; Miller, J.C. *Statistics and Chemometrics for Analytical Chemistry*, 7th ed; Pearson: London, UK, 2020.
45. Shankar, S.S.; Kumara Swamy, B.E.; Mahanthesha, K.R.; Sathisha, T.V.; Vishwanath, C.C. Acetanilide modified carbon paste electrode for the electrochemical detection of dopamine: A cyclic voltammetric study. *Anal. Bioanal. Electrochem.* **2013**, *5*, 19–31.
46. Konstantinova, I.D.; Andronova, V.L.; Fateev, I.V.; Esipov, R.S. Favipiravir and its structural analogs: Antiviral activity and synthesis methods. *Acta Nat.* **2022**, *14*, 16–38. [[CrossRef](#)] [[PubMed](#)]
47. Mehmandoust, M.; Khoshnavaz, Y.; Tuzen, M.; Erk, N. Voltammetric sensor based on bimetallic nanocomposite for determination of favipiravir as an antiviral drug. *Microchim. Acta* **2021**, *188*, 434. [[CrossRef](#)]
48. Allahverdiyeva, S.; Yunusoglu, O.; Yardim, Y.; Senturk, Z. First electrochemical evaluation of favipiravir used as an antiviral option in the treatment of COVID-19: A study of its enhanced voltammetric determination in cationic surfactant media using a boron-doped diamond electrode. *Anal. Chim. Acta* **2021**, *1159*, 338418. [[CrossRef](#)]
49. Mohamed, M.A.; Eldin, G.M.; Ismail, S.M.; Zine, N.; Elaissari, A.; Jaffrezic-Renault, N.; Errachid, A. Innovative electrochemical sensor for the precise determination of the new antiviral COVID-19 treatment Favipiravir in the presence of coadministered drugs. *J. Electroanal. Chem.* **2021**, *895*, 115422. [[CrossRef](#)] [[PubMed](#)]
50. Erşan, T.; Dilgin, D.G.; Kumrulu, E.; Kumrulu, U.; Dilgin, Y. Voltammetric determination of favipiravir used as an antiviral drug for the treatment of COVID-19 at pencil graphite electrode. *Electroanalytical* **2023**, *35*, e202200295. [[CrossRef](#)]
51. García-Miranda Ferrari, A.; Rowley-Neale, S.J.; Banks, C.E. Screen-printed electrodes: Transitioning the laboratory in-to-the field. *Talanta Open* **2021**, *3*, 100032. [[CrossRef](#)]
52. Paimard, G.; Ghasali, E.; Baeza, M. Screen-printed electrodes: Fabrication, modification, and biosensing applications. *Chemosensors* **2023**, *11*, 113. [[CrossRef](#)]
53. Carrara, S.; Baj-Rossi, C.; Boero, C.; De Micheli, G. Do Carbon Nanotubes contribute to Electrochemical Biosensing? *Electrochim. Acta* **2014**, *128*, 102–112. [[CrossRef](#)]
54. Alim, S.; Vejjayan, J.; Yusoff, M.M.; Kafi, A.K.M. Recent uses of carbon nanotubes & gold nanoparticles in electrochemistry with application in biosensing: A review. *Biosens. Bioelectron.* **2018**, *121*, 125–136. [[CrossRef](#)] [[PubMed](#)]
55. Hu, Y.; Fine, D.H.; Tasciotti, E.; Bouamrani, A.; Ferrari, M. Nanodevices in diagnostics. *Wiley Interdiscip. Rev. Nanomed. Nanobiotechnol.* **2011**, *3*, 11–32. [[CrossRef](#)] [[PubMed](#)]
56. Shetti, N.P.; Bukkitgar, S.D.; Reddy, K.R.; Reddy, C.V.; Aminabhavi, T.M. Nanostructured titanium oxide hybrids-based electrochemical biosensors for healthcare applications. *Colloids Surf. B Biointerfaces* **2019**, *178*, 385–394. [[CrossRef](#)] [[PubMed](#)]
57. Bard, A.J.; Faulkner, L.R. *Electrochemical Methods: Fundamentals and Applications*; John Wiley & Sons Inc.: New York, NY, USA, 2001.
58. Gosser, D.K. *Cyclic Voltammetry*; VCH: New York, NY, USA, 1994.
59. Compton, B.R.G.; Banks, C.E. *Understanding Voltammetry*; Imperial College Press: London, UK, 2011.
60. Nicholson, R.S.; Shain, I. Theory of stationary electrode polarography. Single scan and cyclic methods applied to reversible, irreversible, and kinetic systems. *Analyt. Chem.* **1964**, *36*, 706–723. [[CrossRef](#)]
61. Manna, S.; Sharma, A.; Satpati, A.K. Electrochemical methods in understanding the redox processes of drugs and biomolecules and their sensing. *Curr. Opin. Electrochem.* **2022**, *32*, 100886. [[CrossRef](#)]
62. Mohamed, R.M.K.; Mohamed, S.H.; Asran, A.M.; Alshaimi, I.H.; Hassan, H.M.A.; Ibrahim, H.; El-Wakil, M.M. Synergistic effect of gold nanoparticles anchored on conductive carbon black as an efficient electrochemical sensor for sensitive detection of anti-COVID-19 drug Favipiravir in absence and presence of co-administered drug Paracetamol. *Microchem. J.* **2023**, *190*, 108696. [[CrossRef](#)] [[PubMed](#)]
63. Dindar, K.C.; Bozal-Palabiyik, B.; Uslu, B. Development of a Diamond Nanoparticles-based Nanosensor for Detection and Determination of Antiviral Drug Favipiravir. *Electroanalytical* **2022**, *34*, 1174–1186. [[CrossRef](#)]
64. Akça, Z.; Özok, H.İ.; Yardim, Y.; Senturk, Z. Electroanalytical investigation and voltammetric quantification of antiviral drug favipiravir in the pharmaceutical formulation and urine sample using a glassy carbon electrode in anionic surfactant media. *Turk. J. Chem.* **2022**, *46*, 869–880. [[CrossRef](#)] [[PubMed](#)]
65. You, X.-H.; Liu, Y.; Li, Y.-Y.; Zhao, B.; Yang, Y.; Weerasooriya, R.; Chen, X. Sensitive detection of SARS-CoV-2 spike protein based on electrochemical impedance spectroscopy of Fe₃O₄@SiO₂-Au/GCE biosensor. *Adv. Sens. Energy Mater.* **2023**, *2*, 100067. [[CrossRef](#)]
66. Bouali, W.; Erk, N.; Kholafazadehastamal, G.; Naser, M.; Tiris, G. Low-cost voltammetric sensor based on reduced graphene oxide anchored on platinum nanoparticles for robust determination of Favipiravir in real samples. *Diam. Relat. Mater.* **2023**, *131*, 109609. [[CrossRef](#)]

67. Rugar, J.; Aleksić, M.M.; Dobričić, V.; Brborić, J.; Čudina, O. An electrochemical study of 9-chloroacridine redox behavior and its interaction with double-stranded DNA. *Bioelectrochemistry* **2020**, *135*, 107579. [[CrossRef](#)] [[PubMed](#)]
68. Oliveira-Brett, A.M. Electrochemical DNA Assays. In *Bioelectrochemistry: Fundamentals, Experimental Techniques and Applications*; Bartlett, P.N., Ed.; John Wiley & Sons: New York, NY, USA, 2008; pp. 411–442.
69. Galal, A.; Ahmed, Y.M.; Ahmed, M.H.M.; Atta, N.F. Electrochemistry and determination of an antiviral drug at ionic liquids crystals-carbon nanotubes modified glassy carbon electrode. *J. Electrochem. Soc.* **2021**, *168*, 116512. [[CrossRef](#)]
70. Nafisi, S.; Saboury, A.A.; Keramat, N.; Neault, J.F.; Tajmir-Riahi, H.A. Stability and structural features of DNA intercalation with ethidium bromide, acridine orange and methylene blue. *J. Mol. Struct.* **2007**, *827*, 35–43. [[CrossRef](#)]
71. Agafonova, L.; Tikhonova, E.; Sanzhakov, M.; Kostryukova, L.; Shumyantseva, V. Electrochemical studies of the interaction of phospholipid nanoparticles with dsDNA. *Processes* **2022**, *10*, 2324. [[CrossRef](#)]
72. Campos-Carrillo, A.; Weitzel, J.N.; Sahoo, P.; Rockne, R.; Mokhnatkin, J.V.; Murtaza, M.; Gray, S.W.; Goetz, L.; Goel, A.; Schorka, N.; et al. Circulating tumor DNA as an early cancer detection tool. *Pharmacol. Ther.* **2020**, *207*, 107458. [[CrossRef](#)] [[PubMed](#)]
73. Chiorcea-Paquim, A.-M.; Oliveira-Brett, A.M. Electrochemistry of chemotherapeutic alkylating agents and their interaction with DNA. *J. Pharm. Biomed. Anal.* **2023**, *222*, 115036. [[CrossRef](#)] [[PubMed](#)]
74. Bafna, V.; Mischel, P.S. Extrachromosomal DNA in Cancer. *Annu. Rev. Genom. Hum. Genet.* **2022**, *23*, 29–52. [[CrossRef](#)]
75. Salma, U.; Siciliano, G.; Primiceri, E.; Turco, A.; Tarantini, I.; Ferrara, F.; Chiriaco, M.S. Electrochemical sensors for liquid biopsy and their integration into lab-on-chip platforms: Revolutionizing the approach to diseases. *Chemosensors* **2023**, *11*, 517. [[CrossRef](#)]
76. Talapa, J.; Zhaob, J.; Shena, M.; Songa, Z.; Zhoua, H.; Kanga, Y.; Suna, L.; Yua, L.; Zenga, S.; Caia, S. Recent advances in therapeutic nucleic acids and their analytical methods. *J. Pharm. Biomed. Anal.* **2021**, *206*, 114368. [[CrossRef](#)] [[PubMed](#)]
77. Khan, H.; Shah, M.R.; Barek, J.; Malik, M.I. Cancer biomarkers and their biosensors: A comprehensive review. *Tr. Anal. Chem.* **2023**, *158*, 116813. [[CrossRef](#)]
78. Madelain, V.; Nguyen, T.H.T.; Olivo, A.; De Lamballerie, X.; Guedj, J.; Taburet, A.-M.; Mentré, F. Ebola virus infection: Review of the pharmacokinetic and pharmacodynamic properties of drugs considered for testing in human efficacy trials. *Clin. Pharmacokinet.* **2016**, *55*, 907–923. [[CrossRef](#)] [[PubMed](#)]
79. Morawska, K.; Popławski, T.; Ciesielski, W.; Smarżewska, S. Electrochemical and spectroscopic studies of the interaction of antiviral drug Tenofovir with single and double stranded DNA. *Bioelectrochemistry* **2018**, *123*, 227–232. [[CrossRef](#)] [[PubMed](#)]
80. Kostryukova, L.V.; Tereshkina, Y.A.; Tikhonova, E.G.; Khudoklinova, Y.Y.; Bobrova, D.V.; Gisina, A.M.; Morozovich, G.E.; Pronina, V.V.; Bulko, T.V.; Shumyantseva, V.V. Effect of an NGR Peptide on the Efficacy of the Doxorubicin Phospholipid Delivery System. *Nanomaterials* **2023**, *13*, 2229. [[CrossRef](#)] [[PubMed](#)]
81. Graves, D.E.; Velea, L.M. Intercalative Binding of Small Molecules to Nucleic Acids. *Curr. Org. Chem.* **2000**, *4*, 915–929. [[CrossRef](#)]
82. Paleček, E.; Bartošík, M. Electrochemistry of Nucleic Acids. *Chem. Rev.* **2012**, *112*, 3427–3481. [[CrossRef](#)]
83. Bolat, G. Investigation of poly(CTAB-MWCNTs) composite based electrochemical DNA biosensor and interaction study with anticancer drug Irinotecan. *Microchem. J.* **2020**, *159*, 105426. [[CrossRef](#)]
84. Muti, M.; Muti, M. Electrochemical monitoring of the interaction between anticancer drug and DNA in the presence of antioxidant. *Talanta* **2018**, *178*, 1033–1039. [[CrossRef](#)] [[PubMed](#)]

Disclaimer/Publisher’s Note: The statements, opinions and data contained in all publications are solely those of the individual author(s) and contributor(s) and not of MDPI and/or the editor(s). MDPI and/or the editor(s) disclaim responsibility for any injury to people or property resulting from any ideas, methods, instructions or products referred to in the content.